Chemical Science

ROYAL SOCIETY OF CHEMISTRY

EDGE ARTICLE

View Article Online
View Journal | View Issue

Cite this: *Chem. Sci.*, 2025, **16**, 19624

All publication charges for this article have been paid for by the Royal Society of Chemistry

Received 23rd May 2025
Accepted 2nd September 2025

DOI: 10.1039/d5sc03738g

rsc.li/chemical-science

Synthesis of biodegradable vinyl copolymers *via* enforced regular sequence distribution from automated radical ring opening polymerisation

Mengyuan Wen, WeiNian Wong and Tanja Junkers *

A method based on continuous Bayesian optimization of monomer feed in a semi-batch copolymerization is demonstrated that allows countering the composition drift in copolymerizations stemming from disparate reactivity ratios. The method requires online monitoring of the reaction, but requires no prior kinetic knowledge on the copolymerization or any modelling of the polymerizations, making this the first method generally applicable to any copolymerization system to achieve this aim. Copolymerizations between acrylates, methacrylates and styrene are demonstrated to achieve perfectly statistical and homogeneous distributions, and the radical ring opening copolymerisation between a cyclic ketene acetal and methyl methacrylate is showcased as an example of a challenging copolymerization where countering the composition drift results in a completely degradable material, paving a pathway to new sustainable polymers in the future. Next to perfect regulation of the sequence distribution in these copolymers, we also demonstrate how the method can be applied to create non-natural composition drifts in polymers at will.

Introduction

The constant increase in the use of polymer materials made from vinyl monomers is constantly worsening issues associated with plastic pollution.[1] This class of polymers is particularly environmentally unfriendly as chain propagation of these monomers leads to stable all-carbon backbones that are especially persistent in nature.[2] While these backbones provide materials with high toughness, durability and specific beneficial properties, their stability typically outlasts their desired life cycle by far, leading to accumulation of plastic waste in the water, soil and animal bodies.[3] To mitigate the growing accumulation of plastic waste, biodegradable polymers, such as poly(lactic acid) (PLA), polycaprolactone (PCL), and poly(glycolic acid) (PGA), have been developed as alternatives to the conventional vinyl polymers.[4] These materials, synthesized *via* ring-opening polymerization (ROP), aim to address plastic pollution by shortening the life cycle of plastics *via* either recycling or degradation, followed by bio-assimilation by microbes.[5] However, such aliphatic polyesters with high ester content synthesized *via* ROP are associated with limitations in their physical properties,[6] making them more susceptible to fibre damage and thermal degradation during extrusion and injection molding.[7] Therefore, maintaining a low oxygen content in polyesters is crucial to improve the performance of biodegradable polyesters.

Polymer Reaction Design Group, School of Chemistry, Monash University, 17 Rainforest Walk, Clayton VIC 3800, Australia. E-mail: tanja.junkers@monash.edu

As an alternative to classical ring opening polymerization, radical ring opening polymerization (RROP) has regained popularity in recent years to synthesize biodegradable polymers. This subset of ROP utilizes cyclic monomers containing a vinyl or exo-methylene group, such as cyclic ketene acetals (CKAs),[8–12] thionolactones,[13] and a range of macrocyclic monomers.[14–16] These monomers can perform a β-scission ring-opening reaction to incorporate heteroatoms and functional groups onto the main polymer chain upon radical initiation *via* a radical polymerization (RP) mechanism (Scheme S1).[8,17] RROP combines the advantages of RP and ROP, enabling a low concentration incorporation of degradable ester bonds in polymer chains by a relatively mild, simple and efficient reaction mechanism.[18] The unique feature of RROP hereby allows the mixing of polyester units into classical vinyl polymers, thus creating materials that are particularly degradable while largely retaining the properties of their parent vinyl polymers. Among cyclic monomers, CKAs have been the most extensively studied class in RROP since the 1980s, with pioneering work by Bailey[19] and Endo.[20] CKAs' ability to copolymerize with conventional vinyl monomers facilitates the synthesis of a variety of functional macromolecules for diverse applications.[21,22] However, the application of CKAs is often deterred by their limitation of incorporation into the copolymer backbone, both due to the inherent low reactivity and to the competition between their ring-opening and ring-retaining reactions, which likewise limit the number of ester groups being incorporated into the backbone.[17] One CKA that performs well with respect to ring-opening in polymerization is 5,6-benzo-2-methylene-1,3-

dioxepane (BMDO), first introduced by Bailey and coworkers in 1982,[23] which undergoes 100% ring-opening due to radical stabilization by its phenyl ring.[22] Despite its advantages, the low reactivity ratio of BMDO and most CKAs compared to conventional vinyl monomers induces (with the notable serendipitous exception of vinyl ethers)[24] a significant composition drift during copolymerization and compositional heterogenicity in the copolymers, which severely limits their degradability.[25] In consequence, BMDO (and most other CKAs) copolymerization have rather niche applications, and other, more reactive cyclic monomers dominate current research. However, if this hurdle is overcome, then monomers such as BMDO will be the ideal candidates for biodegradable polymer design.

Composition drift results from a disparate reactivity ratio of the comonomers involved in a copolymerization. The statistical distribution of monomer composition can be quantitatively described by using the Mayo–Lewis equation based on the terminal model, as shown in Fig. 1B, which depicts the relative rate of consumption of monomer 1 and 2 (d[M_1] and d[M_2]) regarding their reactivity ratio r_1 and r_2, defined by the propagation kinetics (eqn S(3)). In its mole fraction form, the mole fraction of monomer 1 in the copolymer (F_1 in Fig. 1B) is determined with the molar feed of monomers (f_1 and f_2 in Fig. 1B) and the reactivity ratios of monomers (r_1 and r_2), as described in Fig. 1A.[26,27] In the case of the copolymerization between MMA and BMDO, shown in Fig. 1C, a 20-fold difference in their reactivity ratios is present ($r_{MMA} = 10.05$ and $r_{BMDO} = 0.50$, see Fig. S9); thus, MMA depletes at a much faster rate and produces a divergent comonomer statistical distribution between different copolymer chains, as shown in Fig. 1D. With this distribution, some chains will be fully degradable, and some will be practically non-degradable, removing the advantage that such RROP copolymers in principle possess. To achieve a homogeneous degradation, it is important to develop a uniform sequence distribution in the synthesized copolymer chains. The way to achieve this is to counter the composition drift that is naturally occurring by controlled dosing of the more reactive monomer into the system at an optimized rate during polymerization. This in turn keeps the monomer feed (f_{MMA}) constant throughout the reaction, resulting in a constant copolymer composition (F_{MMA}) and hence sequence regulation as shown in Fig. 1E. As pointed out, such homogeneous statistical distribution is of great importance for the degradability of the synthesized copolymers as the entire polymer can then be readily degraded to oligomers on the nanoscale upon hydrolysis, eliminating the possibilities to generate microplastics. Indeed various methods have been established to control copolymer composition in solution and emulsion copolymerization through manipulation of monomer feed composition to attain a uniform monomer distribution, such as in semi-batch reactors and continuous stirred tank reactors (CSTRs).[28]

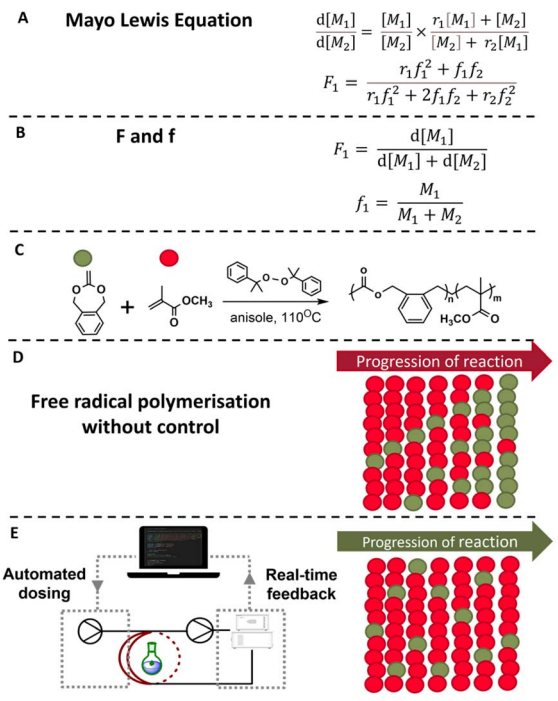

Fig. 1 (A) The Mayo-Lewis equation and (B) the definition of the molar ratio of monomers in copolymer and molar feed of monomers. (C) The copolymerization reaction of interest in this project. (D) Illustration of the monomer distribution along the synthesized polymer chains without copolymer control and (E) illustration of the targeted uniform monomer distribution within copolymers under the control of the automated dosing platform discussed here.

Semi-batch starved feed reactors managed to mitigate composition drift by feeding either only the more reactive monomer or both monomers into the reactor to maintain a constant molar ratio or concentration ratio of M_1 and M_2.[29] For example, Georgiou *et al.* employed the comonomer starved feed strategy in the synthesis of degradable diblock copolymers *via* RROP based polymerization induced self-assembly (PISA) using thionolactone dibenzo-oxepane-5-thione (DOT).[30] Such a method builds upon a pre-calculation of the feeding profile, which demands high accuracy in the mathematical modelling of mass balances, polymer balances, reaction volume, and additional ingredient balances.[31] Due to the non-linearity of the copolymerization profile that arises from gelation, cage effects, and changes in volumetric dynamics and reaction kinetics,[29,31,32] advanced models were developed in engineering process control to mitigate composition drift.[33–35] For example, Rusil *et al.* developed an approach to regulate monomer composition distribution of poly(*N*-vinylimidazole) using the feeding ratio predicted by an optimal monomer addition profile by modelling the individual rate of conversion of monomers.[36] What all available methods have in common is that they require comprehensive kinetic studies, which are usually time-consuming and experiment-specific. The change in reactivities of comonomers corresponding to different reaction conditions, such as monomer concentration, initiator concentration, solvents, and reaction temperature, further aggravates the problem.[37] Thus, such strategies might be applicable to some industrial settings where a specific reaction is repeated indefinitely, yet they all fail when generality and flexibility are required. This project thus aims to replace the need for such complex kinetic studies with a combination of automation,

machine learning (ML) and real-time monitoring techniques. To the best of our knowledge, we herein present the first successful attempt at generalization of the methodology in composition drift control of copolymerization in which no prior knowledge of the reactivity and the specific reaction conditions of the polymerization is required. This will not only provide faster solutions to the issues discussed above, but also open pathways to new biodegradable materials at scale.

ML-based strategies have been widely adopted recently to overcome "the curse of high dimensionality" in the scientific factorial design of experiments (DoE) and industrial chemical process optimization.[38] Different from traditional statistical modelling, ML allows machines to establish a self-learning process to model and adjust the internal parameters based on input values.[39] Bayesian optimization (BO) is a benchmarking ML approach built on a Gaussian Process (GP) model to efficiently solve a bound-constrained single- or multi-objective optimization using an acquisition function.[40] GP models are based on a regression algorithm derived by calculating the confidence intervals of a probabilistic model, featuring easily tuneable hyperparameters.[39] With its built-in algorithm, BO is able to optimize experimental parameter(s) iteratively to fulfil a predetermined objective function, which is usually an expensive "black-box" function, without the requirement of prior knowledge.[41] Recently, the application of BO has gained traction in polymer chemistry and materials science. For example, Weismantel *et al.* developed a BO based platform for synthesizing nanoparticles with targeted sizes.[42] Rubens and Junkers developed an automated flow synthesizer to optimize molecular weight distribution.[43] Similarly, Knox *et al.* successfully designed an automated RAFT polymerization flow synthesizer to maximize monomer conversion while minimizing molar mass dispersity.[44] The composition in copolymers, namely poly(MMA-*co*-styrene), was regulated using BO by Takatsuka *et al.*,[37] though the comonomers' reactivity ratios are relatively close to 1, hence not requiring specific optimization as comonomer and copolymer feed will automatically be close to identical in such a system.

The self-optimization of BO involves constant updates on the GP model based on the real-time progress of, in this case, copolymerization in composition drift control, and exports an optimized decision based on the updated model. This closed loop experimentation approach necessitates the integration of an inline monitoring tool to the setup. The implementation of inline or online NMR,[45] size exclusion chromatography (SEC),[46] and Fourier-transform infrared spectroscopy (FTIR)[47] has been widely established in polymer chemistry to monitor a variety of molecular information *in situ*. Here, we will show how a statistical copolymer with perfect sequence regulation can be synthesized by BO-regulated monomer control in an automated setup integrated with real-time FTIR. Such automation offers the potential to synthesize degradable copolymers with perfectly tuneable copolymer composition, architecture, and degradability performance at will, without the need for redesigning monomer structures to achieve specific reactivities. As we will show, the method is broadly applicable and generalizable and even allows for the synthesis of artificial composition drifts which would not occur in any natural copolymerization.

Results and discussion

Reactor design

An automated semi-batch dosing system regulated by a BO algorithm is employed to mitigate composition drift (see Fig. 2). A batch reactor, preloaded with a mixture of BMDO, MMA and dicumyl peroxide (DCP) in anisole, is prepared under an argon atmosphere to prevent BMDO hydrolysis. Throughout the experiment, both the reactor and MMA dosing vials are degassed with argon *via* a balloon to avoid possible impact from unexpected leakage. The molar ratio of charged BMDO and MMA is adjusted to achieve an initial target f_{MMA} of 0.3, 0.5, and 0.7 (Table 1). In our setup, two pumps are connected to the reactor, one controlling the MMA dosing rate, the other continuously circulating a portion of the reactor content through an inline FTIR system for real-time molar ratio monitoring. The BO algorithm dynamically adjusts the MMA dosing rate based on monomer molar feed to obtain a constant monomer feed at any given time $f_{MMA,t}$. The FTIR peaks used to monitor the molar feed of MMA (1628–1644 cm^{-1}) and BMDO (1672–1680 cm^{-1}) are shown in Fig. 3 with enlarged exact peak ranges. In the reaction with an initial $f_{MMA} = 0.5$, the vinyl peak integration area of MMA gradually diminishes to zero over five hours, whereas the vinyl peak integration area of BMDO decreases at a much slower rate ($X_{MMA} = 100\%$, $X_{BMDO} = 10\%$). To minimize the impact made by the dead volume, the FTIR loop tubing volume is kept as small as possible (264 μL). To minimize the delay in real-time monitoring, a one-minute pause is applied after each dosing to allow for averaging measurements. To ensure the accuracy of peak integration area calculation, the five latest FTIR scans are collected every minute by setting the flow rate of the FTIR loop as 1.32 mL min^{-1} (5 × 264 μL). $f_{MMA,t}$ is determined by averaging the vinyl peak integration area of MMA ($\bar{A}_{MMA}$) and BMDO ($\bar{A}_{BMDO}$) based on the Beer–Lambert law, that the FTIR adsorption is correlated with the concentration of monomers.

The operation of the BO algorithm necessities a set of training data to establish the first model. In this project, the BO algorithm initializes its learning model with four sets of predefined training data, obtained from MMA dosing rates of 0, 20, 25, and 30 μL min^{-1}. Although BO algorithms are usually trained with random data, these initial dosing rates are selected to keep the initial training dosing of MMA at a lower level while maintaining a relatively broad parameter space in the training data. At an earlier stage of this project, ten sets of data instead of four were used; however, it was found that four sets of initial points are sufficient to generate a good initial model. Each input generates a f_{MMA} output in real time, which is compared to the target $f_{MMA,target}$ using an objective function. The gap, the absolute difference between $f_{MMA,t}$ and $f_{MMA,target}$ is described in eqn (1).

$$\text{gap} = |f_{MMA,t} - f_{MMA,target}| \quad (1)$$

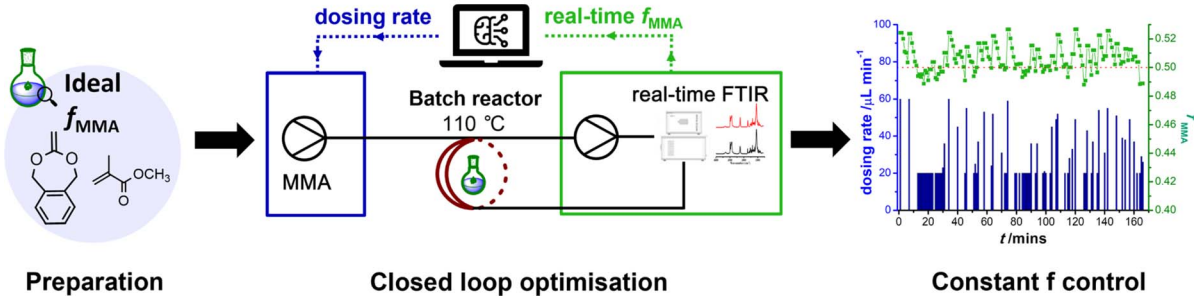

Fig. 2 Schematic overview of the used experimental setup, featuring a main reactor compartment connected to an automated monomer dosing control pump, regulated by the feedback from real-time FTIR. The system uses a Bayesian self-learning algorithm to achieve a constant feed control over time.

Table 1 An overview of the molar ratio of monomers and the initiator during the copolymerization between BMDO and MMA to control different target f_{MMA}

Target f_{MMA}	n_{MMA}/mol	n_{BMDO}/mol	n_{DCP}/mol	c_{MMA}/mol L^{-1}	c_{BMDO}/mol L^{-1}	$\overline{f_{MMA}}$	SD (f_{MMA})
0.3	1.69×10^{-3}	3.95×10^{-3}	1.13×10^{-3}	1.65	3.85	0.339	2.5×10^{-2}
0.5	3.78×10^{-3}	3.78×10^{-3}	1.51×10^{-4}	2.62	2.62	0.507	9.7×10^{-3}
0.7	1.13×10^{-2}	4.56×10^{-3}	3.04×10^{-3}	2.29	1.50	0.709	6.5×10^{-3}

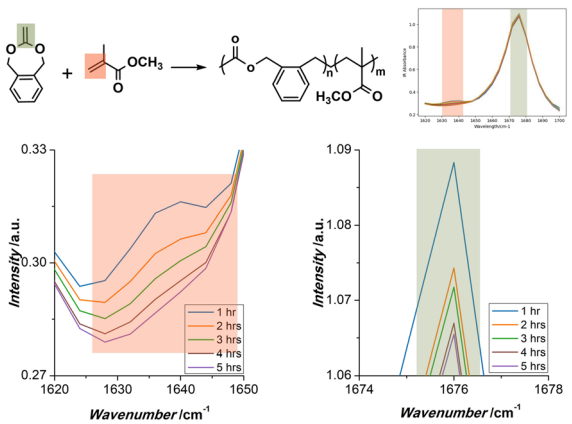

Fig. 3 FTIR absorption ranges selected for monitoring the monomer molar ratio in BMDO/MMA radical copolymerization starting at 1 : 1 molar ratio in 50% wt anisole at 110 °C over 5 hours resulting in 100% MMA conversion and 10% BMDO conversion.

It is important to note that while in this example we integrated the characteristic peak areas, thus directly obtaining the true f_{MMA}, for the experiment it is not important that the peak areas actually represent the true monomer feed ratio, as long as the change in areas is correlated with the change in the feed ratio and the initial feed ratio at the start of the experiment is known. This simplifies the approach largely, as a clear separation of vibrational bands may not always be given for specific copolymerization systems.

During each iteration of flow rate optimization, an optimized dosing rate is generated based on the current GP model, resulting in a new f_{MMA} result. The newly obtained (dosing rate, gap) pair is incorporated into the GP model and further processed by an acquisition function (the Monte Carlo Expected Improvement function) to explore the space to minimize the outcome of the objective function, creating a self-learning loop throughout the course of polymerization. To prevent uncontrolled increases in MMA concentration within the reactor, multiple experiments with different MMA dosing rate boundaries are conducted (20–40, 20–60, 20–100, 20–120, and 20–200 μL min^{-1}). Due to the pump's minimum dosing rate of 20 μL min^{-1}, the lower boundary is set at 20 μL min^{-1} by adding an additional IF condition in the guiding Python script to allow the dosing rate to be set to 0 when the real-time f_{MMA} exceeds target f_{MMA} (Fig. S5). It is further observed that the increases in f_{MMA} become too sharp, *i.e.*, a larger standard deviation in control, when the upper limit of the boundary is set over 100 μL min^{-1}. Therefore, the upper limit of the boundary is set as 60 μL min^{-1} to ensure a stable and flexible regulation of the increase in f_{MMA}. Consequently, the boundary of the MMA dosing rate is constrained within the range of 20 to 60 μL min^{-1}. The details of the reactor setup can be found in the SI (see Fig. S1 and S2).

f control

The effectiveness of the automated dosing platform across different copolymerization systems is demonstrated in Fig. 4A for the copolymerization between BMDO and MMA in anisole, initiated by DCP at 110 °C, with an initial $f_{MMA} = 0.5$. In the uncontrolled system, f_{MMA} drops from 0.5 to 0.09 over 100 minutes, representing the natural composition drift for this monomer pair at the given temperature. However, with the automated dosing control turned on, f_{MMA} is successfully maintained at an average of 0.507 with a standard deviation of 0.0967 (see Table 1 and S2). Fig. 4B illustrates the change in f_{MMA} over 180 minutes for copolymerization targeting different

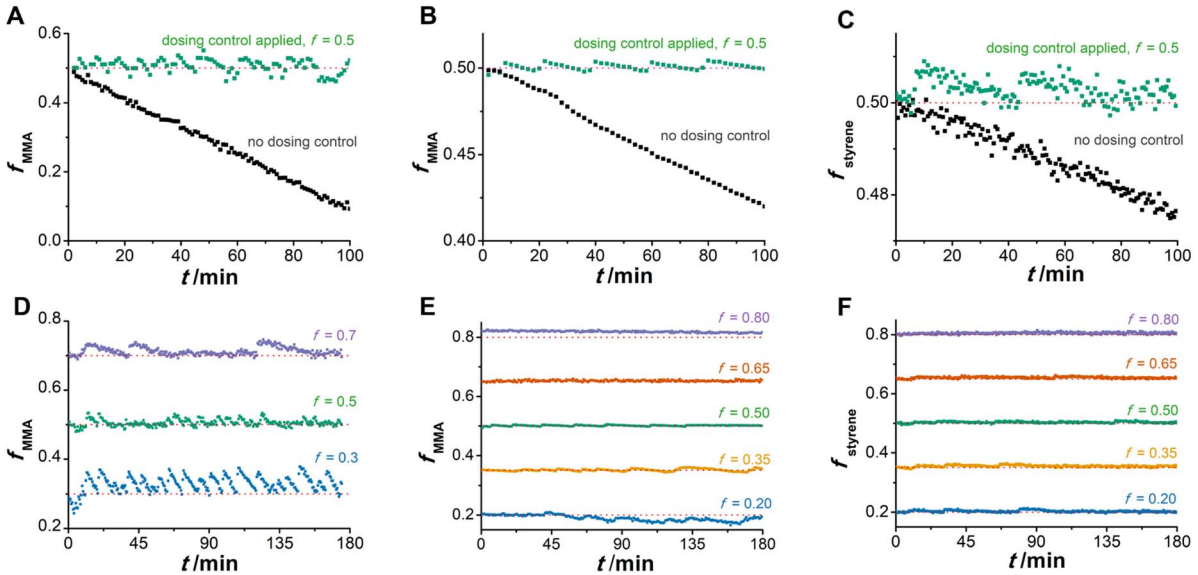

Fig. 4 The change in f_{MMA} without dosing control and its stabilized dosing control at $f_{MMA} = 0.5$ in the BMDO/MMA system at 110 °C with a starting concentration of $c_{BMDO} = c_{MMA} = 2.62$ M in 50% wt anisole is demonstrated in (A). (B) The f_{MMA} change in the BA/MMA system at 60 °C with a starting concentration of $c_{BMDO} = c_{MMA} = 2.85$ M in 50% wt toluene. (C) The control in the styrene/BA system at 60 °C with a starting concentration of $c_{BA} = c_{Styrene} = 2.14$ M. (D) The control of f_{MMA} at 0.3, 0.5, and 0.7 in the BMDO/MMA system. (E and F) The control of f_{MMA} and $f_{styrene}$ at 0.2, 0.35, 0.5, 0.65, and 0.8 in MMA/BA and BA/styrene systems.

f_{MMA} (0.3, 0.5, and 0.7), each corresponding to an ideal initial F_{MMA} of 0.71, 0.88, or 0.95 respectively, which can be translated to a molar composition of MMA to BMDO of approximately 2.5 : 1, 7.4 : 1, or 20 : 1. The yielded copolymers are further characterized with SEC and NMR (see Fig. S10 and S11). While the dosing control itself does not require prior kinetic knowledge, the relationship between the monomer feed f_{MMA} and the copolymer composition F_{MMA} is obviously only established *via* the Mayo–Lewis equation. Thus, from the reaction carried out in the absence of dosing, we determined the reactivity ratios ($r_{BMDO} = 10.05$ and $r_{MMA} = 0.50$; see Fig. S8 and S9) in agreement with the literature. From this knowledge, it is possible to target specific F_{MMA}.

One can see in Fig. 4 that f_{MMA} fluctuates slightly, exhibiting a characteristic 'hill-like' pattern, increasing with MMA dosing before gradually decreasing back to the target value. The system rarely undershoots the target because an IF condition in Python script is applied to trigger an immediate dosing when the real-time f_{MMA} is below the target, leading to an averaged f_{MMA} slightly above the target. The fluctuations are more pronounced for target $f_{MMA} = 0.3$ compared to 0.5 and 0.7, due to their lower initial concentration of MMA. In small-scale reactors with low initial MMA concentrations, even dosing MMA at the lowest dosing rate (20 μL min^{-1}) can result in significant fluctuations in f_{MMA}. However, this fluctuation can be compensated for by increasing the overall reaction volume, and by decreasing the dosing intervals (see Fig. S12). Furthermore, the dosing frequency is found to be higher in the early stage of copolymerization, corresponding to a higher polymerization rate due to higher overall monomer concentration. Unlike other BO based optimization studies in polymer chemistry, which primarily optimize reaction conditions to achieve specific polymer properties, such as molecular weight distributions (MWD),[44,48] this study continuously applies BO throughout the entire experimentation to maintain a constant composition. This approach provides more opportunities to apply BO for real-time polymer optimization in the polymerization process.

To broaden the scope of our system, and to probe the versatility of the used algorithms, we applied the same methodology in the following section to different copolymerization systems with disparate reactivity ratios. We namely tested butyl acrylate-BMDO and styrene-BMDO polymerization and successfully achieved similarly good comonomer feed regulation to that with MMA (see Fig. S10 and S11). Then, we turned to non CKA systems, and studied butyl acrylate (BA)-methyl methacrylate (MMA) ($r_{MMA} = 1.87$ and $r_{BA} = 0.29$)[49] and styrene-BA copolymerization ($r_{styrene} = 0.86$ and $r_{BA} = 0.21$).[50] A comparison between the f_{MMA} change over time in a system with and without dosing control for the BA/MMA copolymerization is shown in Fig. 4C with an initial $f_{MMA} = 0.5$ (Table S3). The copolymerization reactions are conducted with AIBN as initiators in toluene at 60 °C (Tables 1 and S2). In the uncontrolled system, f_{MMA} decreased from 0.5 to 0.42 over 100 minutes. By applying the dosing control, f_{MMA} is kept at a mean value of 0.496, with a standard deviation at 0.0053. Fig. 4D presents the change in f_{MMA} over time for five target f_{MMA}, 0.2, 0.35, 0.5, 0.65, and 0.8 in the BA/MMA copolymerization system. Similar to the BMDO/MMA system, each set of data shows a recurring pattern of increase and decrease in f_{MMA}, but to a lesser extent, since reactivity ratios between BA and MMA are less different than those in the BMDO system. The wave-like pattern in the composition, especially at lower f, is however, mostly a result of the applied lab-oriented setup where the lowest possible pump rate determines the extent of this fluctuation and no overall

drawback of the methodology. When scaled up and moving to a flowrate regime that allows the pumps to have more variability, the wave-like pattern almost entirely disappears (see the SI for details).

The copolymerization between styrene and BA was conducted in toluene at 60 °C with AIBN as the initiator. Fig. 4E presents a comparison of the change in f_{styrene} with and without dosing control, both starting with an initial $f_{\text{styrene}} = 0.5$. In the uncontrolled system, f_{styrene} declined from 0.5 to 0.47 over 100 minutes, whereas f_{styrene} was kept at an average of 0.503 by adopting dosing control, with a standard deviation of 0.0031. The evolution of f_{styrene} during styrene/BA copolymerization over 180 minutes is depicted in Fig. 4F, targeting $f_{\text{styrene}} = 0.2$, 0.35, 0.5, 0.65, and 0.8. The observed f_{styrene} "bumps" were even smaller compared to that in BA/MMA copolymerization, again due to a narrower difference in styrene/BA reactivity ratios.

These results show that the same algorithm can be successfully applied to a broad variety of copolymerization with good success, thus allowing the elimination of copolymerization gradients in reactions, and allowing the general production of homogeneously distributed statistical copolymers. For the BMDO system this means that polymers will be uniformly biodegradable (for preliminary degradation experiments, see the SI), yet many other applications can also be envisioned where such control will prove to be useful.

Gradient *f* control

With the high success of the automation, we realized that the methodology not only allows the removal of naturally occurring composition drifts. It can also be used to create artificial composition drifts. In radical copolymerization this may not be desirable, but when combined with reversible deactivation radical polymerization, such creation of artificial drifts can be used to design specific gradient copolymers. Thus, in the last step we explored whether this platform can be in principle used to control a non-natural gradient change in the molar composition of a polymer in BA/MMA copolymerization as a model case. Experiments are conducted in toluene at 60 °C, starting with an initial $f_{\text{MMA}} = 0.5$. Unlike previous experiments, a different objective function is applied to create a constant changing gradient in f_{MMA} over time by using eqn (2) and (3).

$$\text{gap} = |k_{\text{MMA},t} - k_{\text{MMA,target}}| \quad (2)$$

$$k_{\text{MMA}} = \frac{f_{\text{MMA},t} - f_{\text{MMA},t_0}}{t - t_0} \quad (3)$$

In which k_{MMA} represents the selected gradient of the change in f_{MMA}, f_{MMA,t_0} and $f_{\text{MMA},t}$ stands for the f_{MMA} calculated $t = t_0$ and t, and gap again stands for the variable to be minimized in the BO. The results for this targeted gradient control are depicted in Fig. 5.

The gradient in the change of f_{MMA} represents the rate of incorporation of MMA into the copolymer backbone by assuming that the rate of MMA incorporation equals the consumption of MMA. Three rates of incorporation of MMA targets are tested, each representing an increase of f_{MMA} from 0.5 to 0.6 (target $k_{\text{MMA}} = 0.001$), 0.7 (target $k_{\text{MMA}} = 0.0015$) and 0.8 (target $k_{\text{MMA}} = 0.002$) over three hours. To accommodate the gradient control, the boundaries of the MMA dosing rate are expanded to 20–200 μL min^{-1}. During the 180 minute BA/MMA copolymerization, f_{MMA} exhibits a 'step-like' pattern where each rise corresponds to an intensive MMA dosing phase. The subsequent decreases further help fine-tune the trajectory of the f_{MMA} increase to align with the target slope. A larger deviation from the target slope is observed in the first 120 minutes of the experiments, while improved alignment with the linear fit is achieved thereafter due to the self-improvement attribute of the BO algorithm applied. In any case, the data show nicely that the MMA content in the polymers increases with time under the gradient control that is applied, a result that is completely opposite to the natural composition drift (about a 10% decrease in MMA content over the course of 100 minutes, see Fig. 4). Increases in f_{MMA} content by roughly 10, 15 or 20% over 3 h reaction time are almost effortlessly achieved. Unfortunately, the real-time conversion of monomers could not be accurately determined in the present example due to considerable peak overlaps, hence preventing to date a precise correlation of time with overall monomer conversion. Nonetheless, the excellent control that is achieved over the time evolution of the gradient shows that practically any gradient, no matter how far off from the natural composition drift can be achieved, thus unlocking an enormous synthetic potential towards future development of a multitude of new polymer systems.

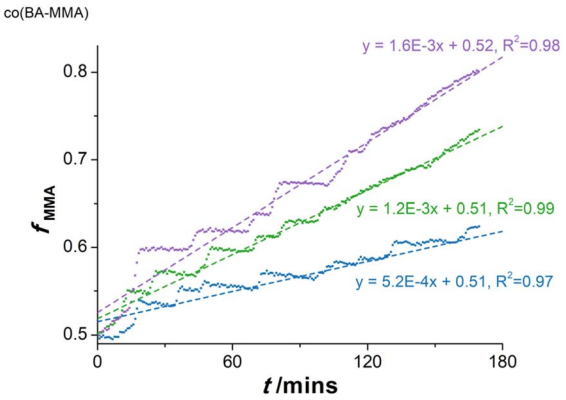

Fig. 5 Artificial gradient control in copolymerization of BA and MMA showing different rates of incorporation of MMA into the copolymer at three different slopes.

Conclusions

With a comparatively simple approach, we achieved the manipulation of the composition drift that naturally occurs in most copolymerizations. This allows the synthesis of polymers with virtually any composition with a steady distribution of sequences over the entire polymerization. This mitigates the issue that in most copolymerizations, a change in copolymer composition occurs over time, compromising the desired properties of the residual material. This is especially a problem in sustainable polymer synthesis, where specific degradable groups are introduced *via* copolymerization and where

composition drift causes parts of the obtained polymer to remain essentially non-degradable. The method we describe is versatile, allows the variation of the copolymer composition *F* at will, and can even be used to create non-native compositions drifts. The latter will be of high significance in RDRP copolymerization as it can be used to create gradient copolymers that until today have not been available.

Notably, the machine-learning based method we use is not dependent on any prior kinetic knowledge or complex modelling to achieve the desired results, making the method universally applicable to a broad range of copolymers and applications. Future work will focus on sustainable polymers and the exploitation of the non-natural gradients that can be achieved.

Author contributions

M. W. and W.W. contributed equally to this work. T. J. supervised this project. The manuscript was written through contributions of all authors. All authors have given approval to the final version of the manuscript.

Conflicts of interest

There are no conflicts to declare.

Data availability

All software code used in this work is available from **https://github.com/PRDMonash/automated_dosing_composition_drift_control.git**. All data produced in this work can be found at **https://doi.org/10.26180/28908686.v4**.

Supplementary information: detailed synthetic procedures, spectra, and characterisation results. See DOI: **https://doi.org/10.1039/d5sc03738g**.

Acknowledgements

Funding from the Australian Research Council in the form of project DP240100120 and IC190100034 is kindly acknowledged.

Notes and references

1 A. T. Williams and N. Rangel-Buitrago, *Mar. Pollut. Bull.*, 2022, **176**, 113429.
2 J. M. Millican and S. Agarwal, *Macromolecules*, 2021, **54**, 4455–4469.
3 M. MacLeod, H. P. H. Arp, M. B. Tekman and A. Jahnke, *Science*, 2021, **373**, 61–65.
4 C. I. A. L. Fuente, B. C. Maniglia and C. C. Tadini, *Packag. Technol. Sci.*, 2022, **36**, 122–130.
5 A. Samir, F. H. Ashour, A. A. A. Hakim and M. Bassyouni, *npj Mater. Degrad.*, 2022, **6**, 112068.
6 T. Nguyen and M. Bavarian, *Polymer*, 2023, **275**, 125866.
7 L. T. Lim, R. Auras and M. Rubino, *Prog. Polym. Sci.*, 2008, **33**, 820–852.
8 Y. Deng, F. Mehner and J. Gaitzsch, *Macromol. Rapid Commun.*, 2023, **44**, 2200941.
9 G. Hedir, C. Stubbs, P. Aston, A. P. Dove and M. I. Gibson, *ACS Macro Lett.*, 2017, **6**, 1404–1408.
10 Y. Deng, A. Frezel, F. Mehner, P. Friedel and J. Gaitzsch, *Polym. Chem.*, 2023, **14**, 4275–4281.
11 Y. Du, L. Ren, J. Sloan, S. Chong, A. Lamprou, Y. Du and E. B. Coughlin, *Polymer*, 2024, **309**, 127444.
12 S. Ganda, Y. Jiang, D. S. Thomas, J. Eliezar and M. H. Stenzel, *Macromolecules*, 2016, **49**, 4136–4146.
13 B. Luzel, N. Gil, P. Désirée, J. Monot, D. Bourissou, D. Siri, D. Gigmes, B. Martin-Vaca, C. Lefay and Y. Guillaneuf, *ChemRxiv* 2023, preprint, DOI: **10.26434/chemrxiv-2023-zrcgd**.
14 J. M. J. Paulusse, R. J. Amir, R. A. Evans and C. J. Hawker, *J. Am. Chem. Soc.*, 2009, **131**, 9805–9812.
15 L. P. D. Ratcliffe, C. Couchon, S. P. Armes and J. M. J. Paulusse, *Biomacromolecules*, 2016, **17**, 2277–2283.
16 Y. Gao, V. I. Böhmer, D. Zhou, T. Zhao, W. Wang and J. M. J. Paulusse, *J. Control*, 2016, **244**, 375–383.
17 A. Tardy, J. Nicolas, D. Gigmes, C. Lefay and Y. Guillaneuf, *Polym. Chem.*, 2017, **8**, 5139–5147.
18 T. Pesenti and J. Nicolas, *ACS Macro Lett.*, 2020, **9**, 1812–1835.
19 W. J. Bailey, S.-R. Wu and Z. Ni, *Makromol. Chem.*, 1982, **183**, 1913–1920.
20 T. Endo, H. Fukuda and M. Hirota, *J. Am. Chem. Soc.*, 1984, **106**, 4035–4036.
21 M. R. Hill, T. Kubo, S. L. Goodrich, C. A. Figg and B. S. Sumerlin, *Macromolecules*, 2018, **51**, 5079–5084.
22 S. Kobben, A. Ethirajan and T. Junkers, *J. Polym. Sci., Part A: Polym. Chem.*, 2014, **52**, 1633–1641.
23 W. J. Bailey, *Makromol. Chem.*, 1985, **13**, 171–190.
24 A. Tardy, J.-C. Honoré, J. Tran, D. Siri, V. Delplace, I. Bataille, D. Letourneur, J. Perrier, C. Nicoletti, M. Maresca, C. Lefay, D. Gigmes, J. Nicolas and Y. Guillaneuf, *Angew. Chem., Int. Ed.*, 2017, **56**, 16515–16520.
25 A. W. Jackson, S. R. Mothe, L. R. Chennamaneni, A. v. Herk and P. Thoniyot, *Materials*, 2020, **13**, 2325.
26 F. R. Mayo and F. M. Lewis, *J. Am. Chem. Soc.*, 1944, **66**, 1594–1601.
27 M. L. Coote and T. P. Davis, *Copolymerisation kinetics in Handbook of Radical Polymerization*, Wiley, New York, 2002, ch. 5, pp. 263–300.
28 J. P. A. Heuts and B. Klumperman, *Eur. Polym. J.*, 2024, **215**, 113215.
29 T. Fujisawa and A. Penlidis, *J. Macromol. Sci., Part A: Pure Appl. Chem.*, 2008, **45**, 115–132.
30 P. G. Georgiou, T. J. Neal, M. A. Newell, K. S. Hepburn, J. J. S. Tyler, M. A. H. Farmer, P. Chohan, P. J. Roth, J. Nicolas and S. P. Armes, *J. Am. Chem. Soc.*, 2025, **147**, 19817–19828.
31 M. Tirrell and K. Gromley, *Chem. Eng. Sci.*, 1981, **36**, 367–375.
32 A. E. Hamielec, J. F. MacGregor and A. Penlidis, *Makromol. Chem., Macromol. Symp.*, 1987, **10–11**, 521–570.
33 T. Kreft and W. F. Reed, *Macromolecules*, 2009, **42**, 5558–5565.

34 Y. Mohammadi, M. Ahmadi, M. R. Saeb, M. M. Khorasani, P. Yang and F. J. Stadler, *Macromolecules*, 2014, **47**, 4778–4789.
35 G. Gardoni, R. Menegon, M. Sponchioni and D. Moscatelli, *ACS Appl. Polym. Mater.*, 2023, **6**, 616–626.
36 W. Rusli, S. W. B. Tan, A. Parthiban and A. M. v. Herk, *Polymer*, 2022, **247**, 124774.
37 S. Takasuka, S. Ito, S. Oikawa, Y. Harashima, T. Takayama, A. Nag, A. Wakiuchi, T. Ando, T. Sugawara, M. Hatanaka, T. Miyao, T. Matsubara, Y.-Y. Ohnishi, H. Ajiro and M. Fujii, *Sci. Technol. Adv. Mater.: Methods*, 2024, **4**, 2425178.
38 K. C. Felton, J. G. Rittig and A. A. Lapkin, *Chem.: Methods*, 2021, 1.
39 W. Sha, Y. Li, S. Tang, J. Tian, Y. Zhao, Y. Guo, W. Zhang, X. Zhang, S. Lu, Y.-C. Cao and S. Cheng, *InfoMat*, 2021, **3**, 353–361.
40 P. Feliot, J. Bect, E. Vazquez, P. Feliot, J. Bect and E. Vazquez, *J. Global Optim.*, 2017, **67**, 97–133.
41 S. Greenhill, S. Rana, S. Gupta, P. Vellanki and S. Venkatesh, *IEEE Access*, 2020, **8**, 13937–13948.
42 O. Weismantel, L. Weerarathna and T. Junkers, *ACS Appl. Polym. Mater.*, 2025, **7**, 938–947.
43 M. Rubens, J. H. Vrijsen, J. Laun and T. Junkers, *Angew. Chem., Int. Ed.*, 2019, **58**, 3183–3187.
44 S. T. Knox, S. J. Parkinson, C. Y. P. Wilding, R. A. Bourne, N. J. Warren, S. T. Knox, S. J. Parkinson, C. Y. P. Wilding, R. A. Bourne and N. J. Warren, *Polym. Chem.*, 2022, **13**, 1576–1585.
45 M. Rubens, J. V. Herck and T. Junkers, *ACS Macro Lett.*, 2019, **8**, 1437–1441.
46 J. V. Herck, I. Abeysekera, A. L. Buckinx, K. Cai, J. Hooker, K. Thakur, E. V. d. Reydt, P. J. Voorter, D. Wyers and T. Junkers, *Digital Discov.*, 2022, **1**, 519–526.
47 B. Zhang, A. Mathoor and T. Junkers, *Angew. Chem., Int. Ed.*, 2023, **62**, e202308838.
48 M. Rubens and T. Junkers, *Polym. Chem.*, 2019, **10**, 6315–6323.
49 S. G. R. and, A. H. E. Müller and K. Matyjaszewski, *Macromolecules*, 1999, **32**, 8331–8335.
50 H. Jianying, C. Jiayan, Z. Jiaming, C. Yihong, D. Lizong and Z. Yousi, *J. Appl. Polym. Sci.*, 2006, **100**, 3531–3535.